Growth and characterization of reduced and unreduced Rh doped potassium niobate single crystals

Ashutosh Choubey, Max Döbeli, Tobias Bach, G. Montemezzani, Detlef Günther, Peter Günter

Growth and characterization of reduced and unreduced Rh doped potassium niobate single crystals

A. Choubey[a,*], M. Döbeli[b], T. Bach[a], G. Montemezzani[a,1], Detlef Günther[c], Peter Günter[a]

[a]*Nonlinear Optics Laboratory, Institute of Quantum Electronics, ETH Swiss Federal Institute of Technology, ETH Hoenggerberg, 8093 Zurich, Switzerland*
[b]*Institute for Particle Physics, ETH Hönggerberg, 8093 Zürich, Switzerland*
[c]*Laboratory of Inorganic Chemistry, ETH Hönggerberg, 8093 Zürich, Switzerland*

Rh doped potassium niobate single crystals are grown by the high-temperature solution growth (HTSG) method with a melt doping level of 1500 mg/g. The crystals are reduced to different levels by subjecting them to an in situ high-temperature reduction under an oxygen-deficient atmosphere followed by fast cooling. The characterization results indicate a segregation coefficient of slightly less than 1% for rhodium. The high-resolution X-ray diffraction studies reveal only a slight broadening for reduced crystals, indicating that the reduction process does not deteriorate strongly the crystalline perfection. Loss of an oxygen atom by formation of an oxygen vacancy accompanied by releasing two electrons is identified as the most likely defect mechanism for the reduction, which results in a lower valence of Rh in the lattice and appears a strong change in the absorption spectrum. The reduction is also accompanied by a loss of hydrogen that leads to a decrease of the infrared (IR) vibrational bonds associated to the OH complex. Two-wave mixing measurements show that majority charge carriers for highly reduced crystals change from holes in unreduced crystals to electrons in reduced crystals at longer wavelength (>580 nm).

1. Introduction

Potassium niobate, $KNbO_3$ (KN), is a very attractive material for photorefractive applications because of its large electro–optic coefficients and the high photosensitivity and photoconductivity observed in reduced crystals [1–3]. The material is used in non-linear and electro-optics and, in the doped form, in the fields of all optical image manipulation, data processing and beam amplification.

It has been demonstrated earlier that reduction of as grown KN crystals enhances the photorefractive properties of the material. The reduced crystals have a higher and faster photorefractive response than the unreduced ones [3–6]. Oxygen is present in KN as O^{2-} with saturated bonds oriented along the octahedral edges. During reduction, when oxygen is removed from the crystal lattice to form O_2 molecules in the surrounding atmosphere, two oxygen vacancies are created inside the crystal, which act as shallow donors containing two electrons [5]. Crystals may be reduced also through the process of hydrogen loading. O–H bonds are being generated in the crystal lattice at the site of oxygen and one electron is made available [7]. In the KN crystal lattice OH vibrational bonds exist in as-grown samples due to hygroscopic nature of the K_2CO_3, starting

*Corresponding author.
E-mail address: ashu@phys.ethz.ch (A. Choubey).
[1]Present address: Laboratoire Materiaux Optiques, Photonique et Systemes (LMOPS, CNRS UMR 7132) University of Metz and Supelec, 57070 Metz.

material used for crystal growth [8]. Hence, during reduction the movement of oxygen atoms and O–H bonds in the crystal lattice takes place and a transition from p-type to n-type conductivity occurs, which helps to increase the effective densities of the photo active centers (electron donors). There are several methods for reducing KN. These include electro–chemical reduction [9], ion implantation [10], reduction by hydrogen loading [7] and high-temperature gas-induced reduction [5,11].

Reduced Rh doped KN crystals grown in our laboratory have been used as efficient photorefractive materials for the near-infrared (IR) wavelengths [5]. However, details of the crystal growth of such crystals have not been reported. In this article we describe the growth of Rh doped KN single crystals by the high-temperature solution growth (HTSG) method [12]. Reduction of part of the crystals by an in situ high-temperature CO/CO_2 gas treatment was performed. In order to improve and control the photorefractive properties of the material, it is important to investigate the behavior of the crystal with respect to the reduction level. Three crystals were investigated: an unreduced and two crystals with a different level of reduction. A detailed investigation of crystalline perfection, composition and optical absorption spectra shows that reduction affects slightly the crystalline perfection. Small change in oxygen concentration modifies the optical properties of Rh doped KN crystals. A comprehensive characterization of the crystal samples by X-ray diffractometry, Rutherford back scattering (RBS), Laser ablation-inductively coupled plasma mass spectrometry (ICP–MS), absorption spectroscopy for visible and near–IR electronic transitions as well as OH stretching vibrations and two-wave mixing measurements is reported here.

2. Crystal growth, reduction and sample preparation

Rh doped KN single crystals were grown by the top seed solution growth method (TSSG) using a home developed crystal growth system. The latter consists of a furnace of super-Kanthal, the sealed crystal growth chamber and a fine pulling and rotation mechanism with accurate crystal weighing detection mechanism.

The KN powder used for the growth experiments was synthesized by mixing K_2CO_3 (Fluka, Puriss) and Nb_2O_5 (H. C. Starck Gmbh & Co. ultra pure grade) powder heated at 800 °C for 4 h. This process was repeated three times to ensure that solid state reaction of the two powders was complete and the resulting powder was KN. A flux of K_2O-rich melt was prepared by adding an additional amount of K_2CO_3 to the KN powder. In the obtained flux with a composition ratio of K_2O:Nb_2O_5 of 51.5:48.5 a small amount of Rh_2O_3 (Aldrich Chem. Co., 99.8% pure) powder was added to produce 1500 μg/g doped melts. This flux was used for the crystal growth experiments. The crystal pull rate was 0.2 mm/h and a rotation rate of 15 rpm were used. A $[1\,0\,1]_c$ seed orientation was kept for all the crystal growth experiments reported here. Here the subscript c indicates the orientation refers to the high-temperature cubic phase of KN.

Unreduced as-grown crystals are normally cooled down to room temperature with a constant 15 °C/h cooling rate. However, for the reduction of the crystals, a two-step cooling process was adopted. It has been observed previously that if the crystals are cooled very fast in an oxygen-deficient atmosphere, re-oxidation of the sample can be minimized [5,11]. Oxygen vacancies are first produced at the surface of the crystal, which is directly exposed to the low oxygen partial pressure atmosphere. In our case the atmosphere was composed by a CO/CO_2 mixture with a 9:100 volume ratio. These vacancies spread, by diffusion, to the whole crystal volume during the 24 h at which the crystal is kept in the reducing atmosphere. In this stage the crystal was pulled out about 2 cm above the melt, where the temperature is approximately 50 °C lower than that of the crystal growth (1040 °C). After this stage, the crystal was cooled in two steps. In the first step the crystals were allowed to cool down fast until they reached a certain temperature (above the cubic–tetragonal phase transition temperature of KN). The typical cool-down rate in this step was in the order of 200–350 °C/h. In the second step a small cooling rate of 15 °C/h was performed until the crystal reached room temperature. The first step of cooling basically allows to freeze-in the reduction state induced at the high temperature. The level of reduction is therefore critically determined by the gas mixture and by the cooling rate of the first step. In our work we have kept the gas mixture constant; however, the cooling rate in the first step is different to achieve different reduction levels.

Figs. 1(a and b) show photographs of as-grown reduced, and unreduced single crystals of Rh doped KN. The boule ♯122 in Fig. 1(a) is highly reduced, its dimensions are roughly $36 \times 18 \times 11\,mm^3$ and its weight is 25.5 g. In contrast, the crystal shown in Fig. 1(b) is unreduced (♯131) and dark yellow in color. It weights 15.3 g and its dimensions are $30 \times 16 \times 9\,mm^3$. The color of the reduced boule of Fig. 1(a) is dark brown in the center and dark amber at the bottom of the crystal. This indicates that reduction is not uniform throughout the crystal boule. The homogeneity in reduction depends on the doping level of the crystal. It has been observed that for higher doping levels one requires low reduction treatment to obtain homogeneous crystals. Earlier investigations with Fe doped KN [13] indicated that constant and relatively fast cooling rates (40 °C/h) can produce homogeneous reduced crystals for low doped crystals. However, highly doped crystals require a faster cooling rate in the first step of cooling. On the other hand, crystals have a tendency to reoxidize in the cooling. Hence, the central region of the crystal shows a stronger reduction than the bottom part or the edges.

As mentioned above, reduction is strongly affected by the process of cooling of the as grown crystal. In the present investigation we have studied three crystal boules in detail. Two of them were reduced and one was unreduced. Among the reduced crystals, the boule ♯122 is

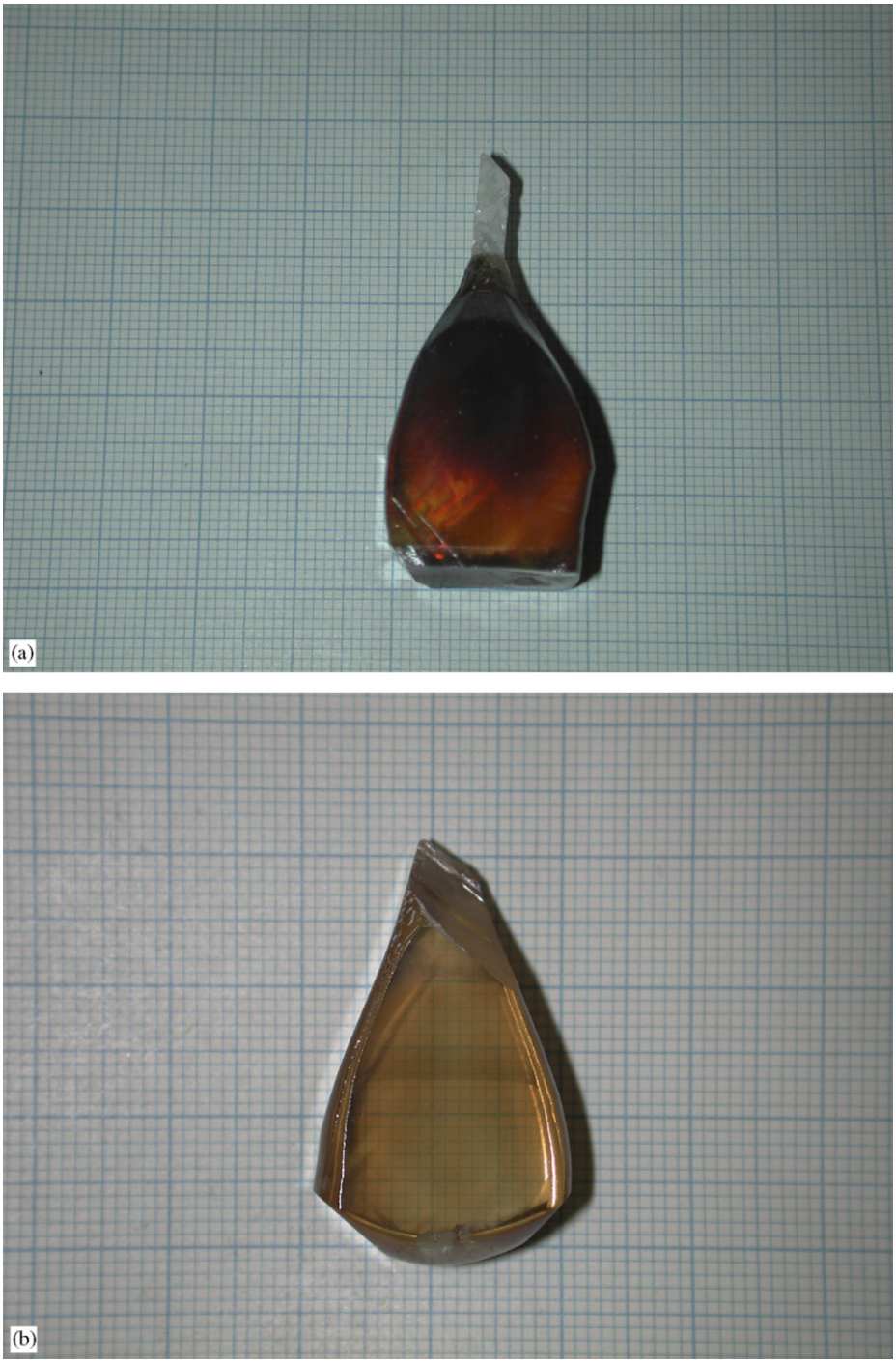

Fig. 1. (a) Highly reduced Rh doped KN crystal and (b) unreduced Rh doped KN Crystal.

highly reduced. For this crystal, the first step of cooling, rate was 350 °C/h temperature. The crystal was allowed to cool at this rate until it reaches 600 °C and then was cooled to room temperature at the slower rate of 15 °C/h. The crystal ♯125 shows a medium degree of reduction. In the first step, this crystal was cooled at a rate of 220 °C/h until 700 °C and was then later cooled further at 15 °C/h. Due to slower initial cooling rate for this crystal the degree of reduction is weaker in the crystal ♯125. The medium reduced crystal is dark amber in color.

2.1. Preparation of specimen crystals

The crystal boules were first lapped with alumina powder and then etched in hydrofluoric (HF) acid at 80 °C for 1 h. By studying the etch pits formation on the *b*-plane of the crystal boule, the *c*-direction (polar axis) of the crystal was determined. The specimen crystals were later oriented by studying Laue X-ray diffraction spots and cut in the wished directions and sizes by using a diamond wire-saw cutter of 40 μm size. The crystals were finally polished with 3 μm

alumina paste and poled in c-direction. The dimensions of the studied samples are: $a \times b \times c = 5.5 \times 1.9 \times 4.5$, $4.2 \times 2.1 \times 5.9$, $6.2 \times 2.4 \times 3.9\,\text{mm}^3$ for sample ♯131 (unreduced), sample ♯125 (medium reduced) and sample ♯122 (highly reduced), respectively.

3. Sample characterizations

The samples obtained by the method described above have been characterized in order to determine the quality of the crystalline lattice, their composition and the level of reduction. For this purpose, high resolution X-ray diffraction (HRXRD), RBS, ICP–MS, absorption spectroscopy and photorefractive two-wave mixing measurements were performed.

3.1. High resolution X-ray diffraction (HRXRD)

HRXRD gives information on the quality of the crystalline lattice. A commercially available X-ray diffractometer (Seifert XRD 3003 PTS-HR) was used for these experiments. The highly monochromatic and collimated CuKα_1 (power: 40 kW, 20 mA) X-ray exiting from the two germanium single crystals taking the role of monochromators was used as a probe beam for the measurements. The X-ray intensity was detected by a scintillation detector.

Fig. 2 shows a typical diffraction curve of the unreduced Rh doped KN crystal sample (♯131) for (0 1 0) diffracting planes. The curve shows a single sharp peak with a half-width of 23 ± 0.5 arcsec. The probe beam size was $15 \times 2\,\text{mm}^2$ for this experiment. Theoretically, the half-width of the diffraction curve for (0 1 0) diffracting plane and CuKα_1 exploring beam is calculated to be 1.55 arcsec by using the plane wave dynamical diffraction theory for X-ray diffraction using the relation [14,15]

$$\Delta\theta = \frac{2r_e\lambda^2 CF_g}{\pi g V_c \cos\theta_B}, \quad (1)$$

where $\Delta\theta$ is half-width, $r_e = 2.82 \times 10^{-15}$ cm is the classical electron radius, $\lambda = 1.54 \times 10^{-8}$ cm is the wavelength of the exploring X-ray beam, C is the polarization factor which is one for symmetrical Bragg reflection, $F_g = 21.0$ is the structure factor, g is the diffraction vector taken as unity for first-order reflection, $V_c = 1.29 \times 10^{-24}\,\text{cm}^3$ is the volume of the unit cell and $\theta_B = 22.8^\circ$ is the Bragg angle.

Keeping in mind the experimental factors such as the divergence of the X-ray beam and the asymmetry in the prepared samples, the observed value of half-width of 23 ± 0.5 arcsec can be considered reasonably close to the calculated values. A rocking curve with half-width of 14 arcsec was observed earlier for a KN crystal grown by the Kyropolus method for (0 1 0) diffraction planes [16]. However, for this experiment a very narrow exploring beam size was used ($0.1 \times 0.1\,\text{mm}^2$) while in our case the beam size was ($15 \times 2\,\text{mm}^2$). As the curve shows a single sharp peak, it indicates that the crystal is free from major defects such as grain boundaries. However, the point defects in the crystals cannot be detected by this measurement.

High resolution X-ray diffraction curves were also recorded for reduced crystals. For medium reduced crystal (♯125) the diffraction curve shows a single sharp peak with a half-width of 26 ± 0.5 arcsec. This half-width is slightly broader than the one observed for the unreduced crystal, suggesting a small deterioration in the crystalline perfection with respect to the unreduced crystal. However, the observation of a single peak in the diffraction curve for the crystal indicates that the reduced crystals are also free from grain boundaries.

Fig. 3 shows the corresponding typical HRXRD curve for the highly reduced crystal sample (♯122). The curve shows a single sharp peak with a half-width of 27 ± 0.5 arcsec. A single sharp peak is observed here, indicating again that the sample is free from grain boundaries. The small broadening of the half-width of the curve with respect to the unreduced and medium reduced crystal suggests that

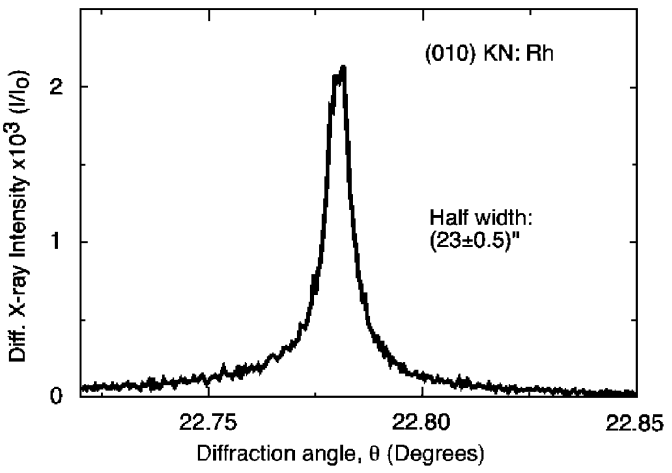

Fig. 2. High resolution X-ray diffraction curve for diffraction at the (0 1 0) plane of unreduced Rh doped KN specimen crystal (♯131).

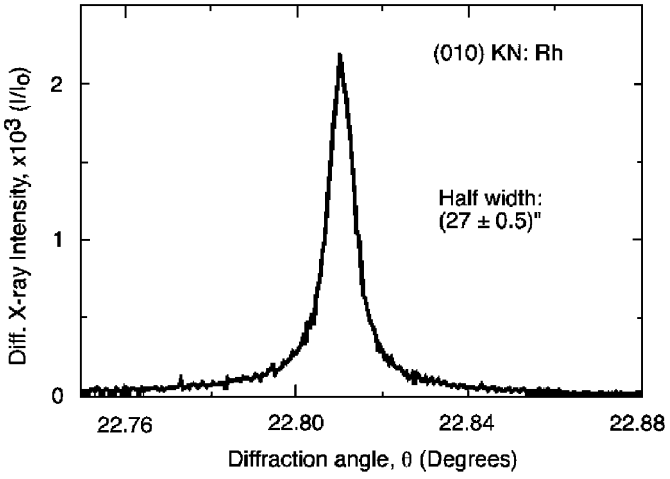

Fig. 3. High resolution X-ray diffraction curve for (0 1 0) diffraction plane of highly reduced Rh doped KN specimen crystal (♯122).

the stronger reduction has slightly affected the crystalline lattice by creation of additional defects. Such an increase of defects is most likely a consequence of the faster cooling process to which the reduced crystals have been subjected (combination of oxygen vacancies and other defects that might have been produced by the thermal stress procedure).

3.2. Rutherford back scattering (RBS)

RBS measurements [17] were performed at the PSI/ETH tandem facility to analyze the composition of the grown crystals as well as their level of reduction. Standard conditions have been applied using a 2 MeV ^{4}He beam and a silicon surface barrier detector under 165°. The height of the K and O edge has been determined by a subtraction procedure. This data have then been analyzed using the RUMP program [18]. The estimated compositions for highly reduced (#122), medium reduced (#125); and unreduced (#131) specimens are calculated and shown in Table 1.

The composition of the specimen crystals are roughly in ratio of 1:1:3 for K, Nb and O, respectively, as expected for KN. Here the measurements are taken with respect to the concentration of potassium and a slight deviation in the composition is within the error limit of the experiment, which is here ±4%. Due to the reduction process applied to the crystals a change in oxygen concentration is expected. However, as seen in Table 1, the difference in oxygen content of the various KN crystals falls under the limit of detection of the technique and could not be detected by RBS measurements. For this reason, non-Rutherford elastic scattering measurements were performed as well. Vizelethy et al. [19] used this technique for profiling oxygen in buried layers of SiO_2 sandwiched between two 300 nm layers of Cu deposited on graphite substrate, and the backscattering yield from the oxygen was enhanced.

Fig. 4 shows the oxygen yield of two specimens of Rh doped KN crystals (unreduced and highly reduced). The experiments were performed with a powder made from these two specimens. From the integrated resonance yield a ratio between the oxygen content of the unreduced to the reduced sample is estimated to be 1.03±0.01. For the medium reduced crystal a negligible change in oxygen concentration has been estimated. The lower concentration in the crystal due to reduction can be understood with the

Table 1
Rutherford backscattering (RBS) measurement of Rh doped KN crystals

Sample number	K	Nb	O	Sample description
# 131	1.0±0.04	0.95±0.04	2.8±0.12	Unreduced
# 125	1.0±0.04	0.99±0.04	3.1±0.12	Medium reduced
# 122	1.0±0.04	1.04±0.04	2.9±0.12	Highly reduced

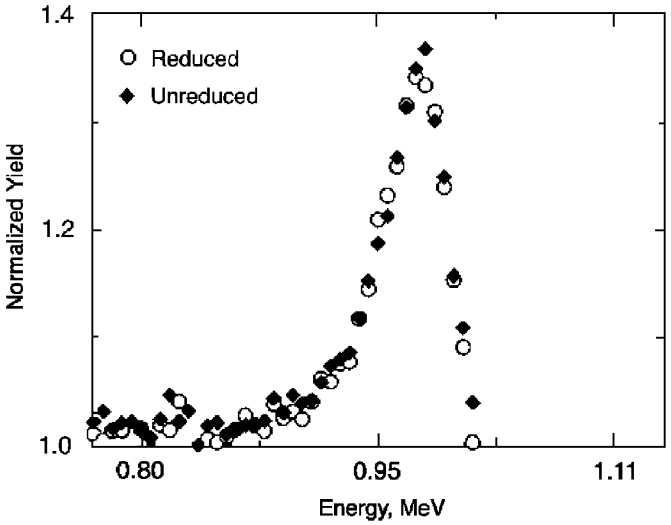

Fig. 4. Rutherford backscattering measurements under oxygen resonance for highly reduced (♯122) and unreduced (♯131) Rh doped KN crystals. The flat background from elements other than oxygen has been subtracted.

following chemical reaction [11]:

$$O_o \rightarrow (1/2)O_2 \uparrow + V_o^{2+} + 2e^-. \quad (2)$$

Here, O_o is the oxygen atom in the crystal, which leaves the crystal lattice as oxygen gas molecule. A vacancy at the oxygen site with +2 charge vacancy (V_o^{2+}) and two electrons are created as a result.

3.3. Laser ablation inductively coupled plasma mass spectrometry (ICP–MS)

The composition of the crystals was determined by using Laser Ablation ICP–MS. This technique is widely used for determination of the major, minor and trace elements as well as isotopic ratios in solids and liquids [20]. The measurements were carried out on a Perkin-Elmer ELAN 6100 DRC ICP-MS coupled to a 193 nm excimer laser ablation system (Geolas M, Lamda Physik, Göttingen, Germany). NIST 610 glass was used as external reference material and Nb was used as internal standard. The concentration of Rh was measured in the crystal at five places for each sample. As an example, for highly reduced sample we obtained 14.6, 13.6, 12.6, 13.0 and 13.3 μg/g for the five locations. The typical variation for the other two crystals is similar. Hence, the rhodium concentration in the samples was determined and calculated as 9.1±0.7, 10.4±1.0 and 13.4±0.8 μg/g for unreduced (♯131), medium reduced (♯125) and highly reduced (♯122) single crystals, respectively. It may be mentioned here that after each crystal growth experiment the additional amount of pure KN material equal to weight of the grown crystal is added in the starting material. Due to this for each new run we start with little less Rh concentration in the crystal than 1500 μg/g. Due to this reason we observe subsequently less Rh in the grown crystal from highly reduced to unreduced

crystal. With these results we believe that segregation coefficient is just slightly less than 1% in the crystal (defined as the ration of concentration in solid and melt in units of weight). The ratio of potassium and niobium for all the three specimen crystals were in agreement with the results obtained by RBS measurements. Unfortunately, the concentration of oxygen could not be directly measured by this technique. The iron concentration in the crystals was below the limit of detection (LOD $< 1.9\,\mu g/g$).

3.4. Optical absorption spectrum

Absorption spectra of the prepared samples were determined from the measured transmission spectra obtained using a Perkin–Elmer $\lambda 9$ spectro-photometer. Fig. 5 shows the measured spectra for the reduced and unreduced Rh doped KN crystals in the wavelength range 450–2000 nm. Light propagation was along the *b*-direction and the polarization along the *a*-direction. Multiple Fresnel reflections were taken into account for calculating the absorption coefficient using the refractive indices given in Ref. [21]. A magnified view of the absorption spectra is shown in the inset of Fig. 5. From the inset one can see that the reduced crystals absorb less in the near-IR wavelength range between 800 and 1100 nm, which is in agreement with the results in Ref. [5]. The unreduced crystal shows a peak around 860 nm which is absent in the reduced crystal. For unreduced and medium reduced crystal no peak is observed in visible range, while for the highly reduced crystal a peak at 480 nm is observed.

Rhodium can exist in the crystal with three valence states Rh^{3+}, Rh^{4+} and Rh^{5+}. Also oxygen vacancies have three possible states, V_o^{2+} (double ionized), V_o^{+} (singly ionized) and V_o^{x} (neutral vacancies). Hence we obtain four ionization energy levels bound to Rh^{3+}–Rh^{4+}, Rh^{4+}–Rh^{5+}, V_o^{2+}–V_o^{+} and V_o^{+}–V_o^{x}. Kröse et al. [22] have suggested that Rh^{4+} has an absorption peak at around 650 nm and Rh^{5+} at around 800 nm for $BaTiO_3$ crystals. In analogy, the peak observed for unreduced KN crystal at 860 nm might be assigned to Rh^{5+}. The corresponding hole photo excitation relation is

$$Rh^{5+} + h\nu \rightarrow Rh^{4+} + \text{hole}, \tag{3}$$

where $h\nu$ indicates the absorbed photon of frequency ν (h is the Planck's constant). The disappearance of this peak in the medium and highly reduced crystals is considered to be due to a gradual reduction of Rh^{5+} to Rh^{4+} and subsequently to Rh^{3+}. In the highly reduced crystal an increase of the absorption in the visible region is observed at 480 nm (Fig. 5). Interestingly, for the crystal with a medium degree of reduction the new absorption band in the visible is not observed. Stevendaal et al. [23] observed a similar peak at 470 nm (= 2.7 eV) for reduced $BaTiO_3$ crystal doped with Rh and Fe in hydrogen environment, but the origin of the peak was not explained. In our case the laser ablation ICP–MS method discribed above did not give evidence for an appreciable iron content inside the crystal.

The reduction level is also influenced by the hydrogen loading in the crystal in form of OH ions, which also indirectly influences the number of oxygen vacancies. Potassium carbonate is a hygroscopic material in nature. Hence, in an as-grown KN crystal hydroxides or hydrates are incorporated inside the crystal lattice. The OH vibrational stretch frequency of hydroxide has been observed in KN spectra at the wavelength of 2850 nm [7,24]. Since the KN crystal boules in the present investigation are reduced in a water free and oxygen-deficient atmosphere, a strong mobilization of the oxygen ions as well as of the protons is expected. Fig. 6 shows IR absorption spectra of the specimens in the range 2800–2900 nm as obtained using a Fourier-transform IR spectrometer. The peak at 2850 nm is observed in all the spectra. By assuming a linear relationship, the area below the absorption peak reflects the concentration of O–H bonds in the sample. It is clear that the O–H bond concentration is the highest in the unreduced crystal and it

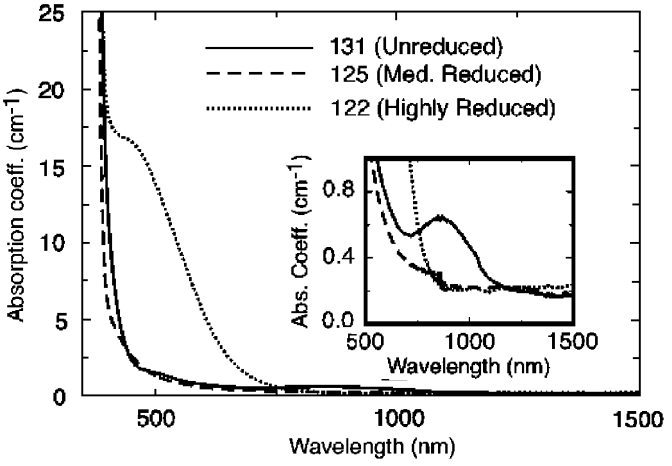

Fig. 5. Absorption spectrum of highly reduced (♯122), medium reduced (♯125) and unreduced (♯131) Rh doped KN crystals. Inset shows magnified graph for absorption coefficient. Here, light propagation is along the *b*-direction and the polarization along the *a*-direction.

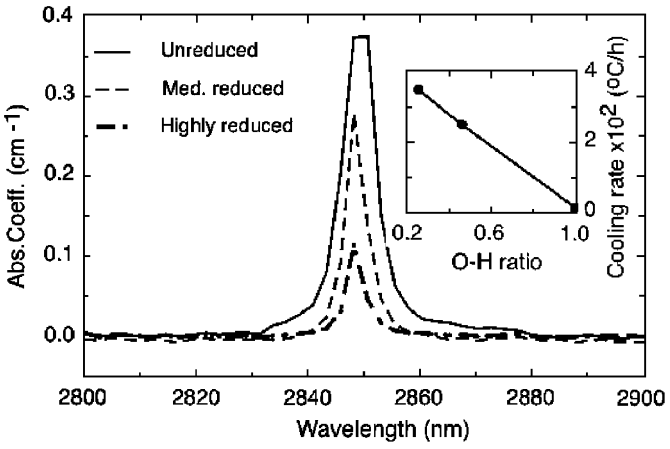

Fig. 6. O–H stretch bond of highly reduced (♯122), medium reduced (♯125) and unreduced (♯131) Rh doped KN crystals. The inset shows the relative concentration of OH vs. post-growth cooling rate of the crystals.

decreases with increasing the degree of reduction. By calculating the areas below the curves in Fig. 6, a ratio of 1:0.46:0.25 in the O–H bond concentrations of unreduced, medium reduced and highly reduced crystals can be roughly obtained. Hydrogen movement from crystal lattice to surrounding atmosphere is expected to follow the reaction [25]

$$2(\mathrm{OH})^{+} \rightarrow \mathrm{H_2O} \uparrow + V_{\mathrm{o}}^{2+} + \mathrm{O_o}. \tag{4}$$

Here, V_{o}^{2+} is an oxygen vacancy (which is doubly positively charged with respect to the corresponding oxygen atom) and $\mathrm{O_o}$ is an oxygen atom left behind at its lattice place. A change of OH ion concentration in response to a reduction process has been observed earlier in other materials, such as in near-stoichiometric lithium niobate crystals [26]. The inset of Fig. 6 shows an empirical relationship between the post-crystal growth initial cooling rate (first phase) and the normalized O–H concentration estimated from absorption spectrum. A clear decrease of O–H bond concentration with increasing cooling rate is observed. As the degree of freezing in the high temperature reduced state depends mainly on the first step of cooling, the final stationary concentration of oxygen vacancies and O–H bonds also depend on this first stage cooling rate and the surrounding atmosphere.

As mentioned earlier, reduction might also be performed in KN crystals within a hydrogen atmosphere [7,23]. In this process O–H bonds are created in the KN lattice. For each O–H bond one electron of the oxygen atom in the crystal lattice is freed, which may reduce the impurity valence. Hence in this process the reduced crystals contain more $\mathrm{OH^-}$ ions than that of the unreduced ones [6]. In contrast, with our reduction technique we have just the opposite. Lower concentration of OH is observed for reduced crystals. Water vapor leaves the crystal and the missing electrons in the created oxygen vacancy are available for reduction of other defects such as Rh.

3.5. Photorefractive two-wave mixing

In order to complement the absorption measurements, we performed photorefractive two-wave mixing experiments using the wavelengths 514, 633 and 780 nm. In Fig. 7 the dependence of the gain as a function of the grating spacing is shown for the wavelength of 780 nm, as an example. The squares and diamonds represent the experimental data for reduced and unreduced KN, respectively. For the diffusion case and assuming an isotropic photo excitation cross-section one can express the stationary two-beam coupling gain coefficient within the weak probe beam approximation as a function of the grating spacing [27]:

$$\Gamma = \frac{4\pi^2 k_{\mathrm{B}} T}{\lambda_{\mathrm{e}}} n_{\mathrm{s}} n_{\mathrm{p}}^2 \frac{\cos 2\Theta_{\mathrm{s}}}{\cos \Theta_{\mathrm{s}}} r^{\mathrm{eff}} \frac{1}{\Lambda\left(1 + (2\pi l_{\mathrm{s}}/\Lambda)^2\right)} \tag{5}$$

where k_{B} is the Boltzmann constant, T is the absolute temperature, n_{S} and n_{P} are refractive indices of the signal

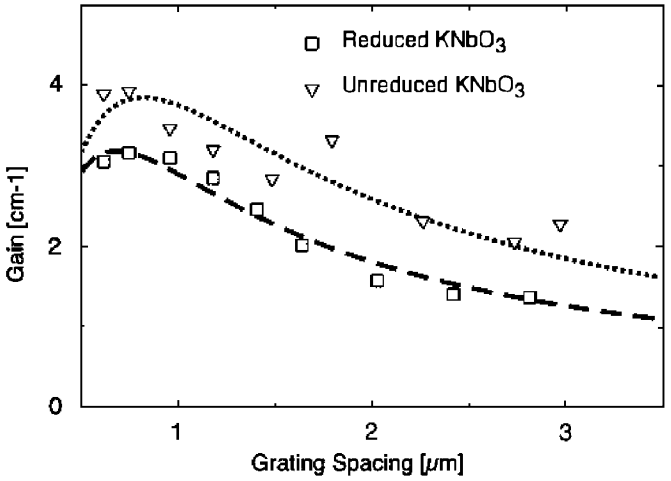

Fig. 7. Photorefractive two-wave mixing gain recorded at the wavelength of 780 nm as a function of the grating spacing. Theoretical calculations for measurements of unreduced (diamonds) and reduced (square) Rh doped KN crystals are shown in dotted and dashed lines, respectively.

Table 2
Dominant charge carriers for reduced and unreduced Rh doped KN crystals

	514 nm	633 nm	780 nm
Crystal # 131 (Unreduced)	Electrons	Holes	Holes
Crystal # 122 (highly reduced)	Electrons	Electrons	Electrons

and the pump beams, Θ_{S} is the angle between the signal beam and the sample normal and r^{eff} is the effective electro–optic coefficient, that includes not only the electro–optic coefficient in the corresponding geometry, but also a reduction factor due to electron–hole competition. $l_{\mathrm{s}} = \sqrt{\varepsilon_{\mathrm{eff}} \varepsilon_0 k_{\mathrm{B}} T/(e^2 N_{\mathrm{eff}})}$ is the Debye screening length, where ε_0 is the electric constant, $\varepsilon_{\mathrm{eff}}$ is the effective dielectric constant, e is the unit charge and N_{eff} is the effective number of traps. The theoretical curves that correspond to our measurements are given with a dashed and dotted line in Fig. 7. From the fitting parameters the effective electro–optic coefficient r^{eff} and the effective concentration of traps N_{eff} were estimated. We obtained r^{eff} of 31 pm/V and 47 ($\pm 5\%$) pm/V and N_{eff} of 8.8×10^{15} and $5.1 \times 10^{15}\,\mathrm{cm^{-3}}$ for the reduced and unreduced sample, respectively.

By knowing the direction of the spontaneous polarization of the crystal, the sign of the electro–optic coefficients and the direction for which light amplification occurs, the sign of the main charge carriers can be determined. Table 2 gives the dominated carriers at the different wavelengths for the different crystals. The expected trend towards electron dominated conduction at progressively longer wavelength upon increasing degree of reduction is confirmed. This is in agreement with earlier observation and is consistent with a progressive filling of the Rh levels upon reduction [5]. However, a conclusive identification of the

origin of the absorption band centered at 480 nm in highly reduced crystals cannot be given on the basis of these two-wave mixing investigations.

4. Conclusions

Rh doped KN crystals were grown by HTSG method and were reduced by the high-temperature gas-induced reduction method under CO/CO_2 atmosphere. A certain inhomogeneity in reduction is observed for highly reduced crystals, while medium reduced crystals are found to be homogeneous. The KN samples are characterized by various methods, HRXRD, RBS measurements, absorption spectroscopy and photorefractive two-wave mixing. HRXRD results show that the grown crystals are free from major defects such as grain boundaries. The continuous broadening of the half-width of HRXRD curves indicates that the crystalline lattice has a slightly larger number of defects due to reduction in forms of point defects and their clusters. RBS measurements performed for the crystals show that the composition of the crystal is close to the stochiometric ratio of 1:1:3 for K:Nb:O. With O-resonance method, a slight decrease in oxygen concentration was observed with reduction. By laser ablation ICP-MS the segregation coefficient for Rh in KN material was measured to be slightly less than 1%. Absorption spectrum studies indicate that unreduced crystals have rhodium in the Rh^{5+} ionization states, which gets gradually charged up to the Rh^{3+} ionization states upon reduction. The unreduced crystal shows a peak at 860 nm while a much lower absorption coefficient in the near IR region of 800–1100 nm wavelength range is observed for reduced crystals. An increase of the absorption constant in the visible region is observed for the highly reduced crystal at 480 nm. Two-wave mixing experiments at the wavelengths 514, 633 and 780 nm show a change of charge carriers from holes to electrons for highly reduced crystals for higher wavelength. The charge carriers are holes for unreduced crystals for the longer wavelength. The study of the OH stretching vibrations shows a significant decrease of OH^- ions concentration upon reduction.

References

[1] P. Günter, Opt. Commun. 11 (1974) 285.
[2] M. Zgonik, C. Medrano, E. Ewart, H. Wüest, P. Günter, Opt. Eng. 34 (1995) 1930.
[3] E. Voit, M.Z. Zha, P. Amrhein, P. Günter, Appl. Phys. Lett. 51 (1987) 2079.
[4] P. Günter, Phys. Rep. 93 (1982) 199.
[5] M. Ewart, R. Ryf, C. Medrano, M. Zgonik. P. Günter, Opt. Lett. 22 (1997) 781.
[6] C. Medrano, M. Zgonik, I. Liakatas, P. Günter, J. Opt. Soc. Am. B 13 (1996) 2657.
[7] A. Förster, H. Hesse, S. Kapphan, M. Wöhlecke, Solid State Commun. 57 (1986) 373.
[8] U. Fluckiger, H. Arend, J. Crystal Growth 43 (1978) 406.
[9] Y. Matsumoto, T. Morikawa, H. Adachi, J. Hombo, Mat. Res. Bull. 27 (1992) 1319.
[10] C. Buchal, Nucl. Instr. Meth. B 166–167 (2000) 743.
[11] J.Y. Chang, C.R. Chinjen, S.H. Duan, C.H. Huang, R.H. Tsou, J.N. Cheng, C.C. Sun, Opt. Commun. 153 (1998) 106.
[12] J. Hulliger, Mater. Res. 26 (1991) 1385.
[13] M.J. Ewart, Ph.D. Thesis, Swiss Federal Institute of Technology, Zurich, Diss ETH No. 12484, 1998.
[14] B.W. Batterman, H. Cole, Rev. Mod. Phys. 36 (1964) 681.
[15] R.V.A. Murthy, M. Ravikumar, A. Choubey, K. Lal, Kh. Lyudmila, V. Shleguel, V. Guerasimov, J. Crystal Growth 197 (1999) 865.
[16] T. Fukuda, Y. Uematsu, T. Ito, J. Crystal Growth 24/25 (1974) 450.
[17] W.K. Chu, J.W. Mayer, M.A. Nicolet, Backscattering Spectrometry, Academic Press, New York, 1978, p. 1.
[18] L.R. Doolittle, Nucl. Instr. Meth. B 15 (1986) 227.
[19] G. Vizelethy, P. Revesz, J. Li, L.J. Matienzo, F. Emmi, J.W. Mayer, in: J.R. Tesmer, C.J. Maggiore, M. Nastasi, J.C. Barbour, J.W. Mayer (Eds.), High Energy and Heavy Ion Beams in Materials Analysis, Materials Research Society, Pittsburgh, PA, 1990, p. 235.
[20] D. Günther, B. Hattendorf, Trends Anal. Chem. 24/3 (2005) 255.
[21] B. Zysset, I. Biaggio, P. Gunter, J. Opt. Soc. Am. B 9 (1992) 380.
[22] H. Kröse, R. Scharfschwerdt, O.F. Schirmer, H. Hesse, Appl. Phys. B 61 (1995) 1.
[23] U.V. Stevendaal, K. Buse, S. Kämper, H. Hesse, E. Krätzig, Appl. Phys. B 63 (1996) 315.
[24] G. Mizell, W.R. Fay, T. Alekel III, D. Rytz, M. Garrett, SPIE Vis. UV Lasers 2115 (1994) 19.
[25] H. Jena, K.V.G. Kutty, T.R.N. Kutty, Mater. Res. Bull. 39 (2004) 489.
[26] K. Kitamura, Youwen-Liu, S. Takekawa, G. Ravi, M. Nakamura, in: Ninth International Conference on Photorefractive Effects, Materials and Devices Trends in Optics and Photonics Series 87, 2003, p. 666.
[27] N.V. Kukhtarev, V.B. Markov, S.G. Odoulov, M.S. Soskin, V.L. Vinetskii, Ferroelectrics 22 (1979) 961.